Lasers in Surgery and Medicine 19:284–298 (1996)

Photodynamic Effects on Human and Chicken Erythrocytes Studied With Microirradiation and Confocal Laser Scanning Microscopy

Karsten König, PhD, Sol Kimel, PhD, and Michael W. Berns, PhD

Beckman Laser Institute and Medical Clinic, UCI, Irvine, California 92715 (K.K., S.K., M.W.B.); Institute for Molecular Biotechnology and Institute of Anatomy II, Friedrich Schiller University, D-07708 Jena, Germany (K.K.); and Department of Chemistry, Technion-Israel Institute of Technology, Haifa 32000, Israel (S.K.)

Background and Objective: **Photodynamic therapy (PDT) of cancers is associated with the destruction of the microvasculature supplying the tumor. The study elucidates the role of red blood cells in PDT-induced vascular injury.**
Study Design/Materials and Methods: **Intracellular accumulation of several photosensitizers in human (non-nucleated) and chicken (nucleated) erythrocytes, as well as photodynamic induced hemolysis were studied using 488 nm laser microirradiation (15 μW) and confocal laser scanning fluorescence microscopy.**
Results: **Cells incubated with anionic hydrophilic compounds $TPPS_4$ and Pd-$TPPS_4$ exhibited no fluorescence before irradiation, but developed strong and sustained fluorescence in the cellular and nuclear membranes following photoinduced membrane damage. In contrast, microirradiation of Photofrin-incubated erythrocytes showed instantaneous fluorescence which decreased due to photodegradation. For the cationic hydrophilic dye methylene blue, significant fluorescence was detected only in the nucleus. Following ALA incubation, large intercellular differences were observed in fluorescence in the red spectral region. Photofrin induced the most efficient hemolysis. Higher radiant exposures were required for lysis of nucleated rather than of non-nucleated red blood cells, except in the case of methylene blue.**
Conclusion: **Laser microbeams were used, for the first time, to study photodynamic cell damage. Erythrocytes were shown to be primary targets in PDT. Damage to red blood cells could be responsible for hemostasis in the vascular bed of a tumor, which was reported by many groups.** © 1996 Wiley-Liss, Inc.

Key words: cellular fluorescence, hemolysis, PDT of red blood cells, microbeam

INTRODUCTION

Vascular effects produced by photodynamic therapy (PDT) have been recognized to play an important role in tumor eradication. It has been demonstrated that in vivo PDT is generally accompanied by vasoconstriction and hemostasis in the vascular bed supplying the tumor with oxygen and nutrients [1]. This leads to tumor necrosis and, ultimately, regression [2]. Vascular effects may be due to injury/hemolysis of red blood cells (RBC) during PDT, which causes swelling, increased rigidity, sludging, clotting, hemostasis [3–7] and, eventually, collapse of the tumor mi-

Accepted for publication May 18, 1995.

Address reprint requests to Michael W. Berns, Beckman Laser Institute and Medical Clinic, University of California Irvine, 1002 Health Sciences Road East, Irvine, CA 92715.

Dr. Berns did not participate in the editorial review of this paper.

© 1996 Wiley-Liss, Inc.

TABLE 1. Chemical and Photophysical Properties of Photosensitizers

Photosensitizer	Solvent	Concentration mg/l	Formula weight	α (488) cm^{-1}	ε (488) $M^{-1}cm^{-1}$
Photofrin	5% glucose	20	?	0.036	?
$TPPS_4$	water	20	1007.7	0.067	3380
Pd-$TPPS_4$	water	20	1114	0.053	2950
MB	water	20	373.9	0.038	710

crocirculation [8,9]. Also, endothelial cell destruction which causes leaking of blood vessels and platelet formation have been suggested [10]. In some cases, direct tumor cell kill was shown responsible for tumor necrosis [11].

The particular blend of vascular and cellular effects in PDT depends on various factors such as physical-chemical properties of the photosensitizer (e.g., hydrophilicity, aggregation, electrical charge), intracellular localization, route of administration (topical or systemic), histopathology, and tumor site [12].

Our goal was to study the interaction of light with single, photosensitizer-incubated erythrocytes. For that purpose we employed the laser microbeam of a confocal laser scanning microscope (CLSM) to induce intracellular photodynamical effects as well as to excite photosensitizer fluorescence. We have investigated human (non-nucleated) and chicken (nucleated) erythrocytes which represent a convenient model for studying PDT-induced changes on the cell membrane and nucleus. The kinetics of hemolysis was monitored by transmission and fluorescence measurements. In addition, intracellular accumulation of photosensitizers in RBC, and PDT-induced changes in fluorescence patterns, were investigated at selected time intervals by confocal fluorescence imaging. The internal Ar^+-ion laser of the CLSM at 488 nm served as the microirradiation source to induce photodynamic hemolysis, as a source for 3-D fluorescence imaging, and for monitoring the kinetics of lysis by bright-field transmission and fluorescence microscopy.

MATERIALS AND METHODS

Photosensitizers

Photosensitizers were selected to cover a range of physical-chemical characteristics. Stock solutions were prepared in phosphate based saline (PBS) (0.9% NaCl, pH 7.4; Sigma, St. Louis, MO) and kept in the dark at 4°C.

Photofrin is a multicomponent preparation containing hydrophobic constituents (Porfimer sodium; Quadralogic, Vancouver, Canada); tetraphenylporphine tetrasulfonate ($TPPS_4$) (Porphyrin Products, Logan, UT) and methylene blue (MB) (Sigma) are, respectively, anionic and cationic hydrophilic compounds; the palladium derivative Pd-$TPPS_4$ (Mid-Century, Posen, IL) is a hydrophilic compound characterized by long-lived fluorescence and phosphorescence [13]; and 5-amino levulinic acid (ALA) (Deprenyl USA, Denville, NJ) is a precursor for protoporphyrin IX (PP IX) biosynthesis [14,15]. The chemical and photophysical properties of these photosensitizers are listed in Table 1.

To obtain photophysically comparable results for the different photosensitizers, stock solutions were chosen to have identical optical density at 488 nm, compared to Photofrin at a concentration of 20 μg/ml in a 1 cm cuvette (A = 0.036). For PDT, a tenfold dilution with PBS was used as a final concentration. For fluorescence measurements and confocal fluorescence imaging, concentrations of 10 μg/ml were used. For ALA, a concentration of 1 mg/ml was chosen arbitrarily.

Sample Preparation

Peripheral human blood was freshly drawn from a finger of a healthy donor, diluted in PBS and a drop of 0.1% heparin added. After incubation in the dark (up to 2 h) with photosensitizer at 37°C, the washed (by twice repeated sedimentation for 5 min, followed by removal of supernatant and resuspension in PBS) or unwashed human red blood cells (HRBC) were introduced into a Rose chamber prior to irradiation. Chicken blood (0.25 ml) was obtained by venipuncture from the wing vein of a 1-year-old white Leghorn chicken and 0.05 ml 0.1% heparin added; in all subsequent procedures, chicken red blood cells (CRBC) were treated in the same way as HRBC.

Instrumentation

The confocal laser scanning microscope (CLSM, Model Axiovert 135M, Zeiss, Germany) was used simultaneously for irradiation of RBC

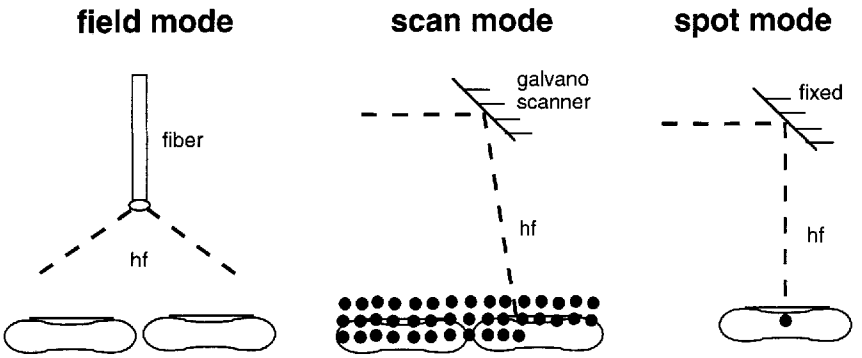

Fig. 1. Schematic representation of irradiation modes.

and measuring morphologic changes by transmission and fluorescence microscopy. The temporal evolution of RBC fluorescence was monitored in the standard as well as in the confocal configuration. In the confocal mode, an erythrocyte is "sliced" into n slices of a chosen thickness; each slice is scanned sequentially to obtain 3-D fluorescence images.

The internal Ar^+-ion laser of the CLSM served as a light source at 488 nm for transmission and fluorescence imaging and for inducing hemolysis. The laser output in the focal plane of the brightfield objective (100X, numerical aperture 1.3) was 15 μW as measured with a power meter (Model 1815-C, equipped with 818 UV detector, Newport Corporation, Irvine, CA).

In addition, an external Ar^+-ion laser (Coherent, model: innova 100), tuned to 488 nm, was used for inducing hemolysis.

Irradiation

Three modes of irradiation were employed to induce photodynamic hemolysis (Fig. 1):

(i) "field" mode; an external Ar^+-ion laser (488 nm, power P = 100 mW) coupled to an optical fiber irradiated an area of diameter Δ = 4 mm, covering the whole field of view (about 128 × 128 μm^2), during time t. This mode closely resembles irradiation conditions in standard PDT experiments and served as a reference for the other two modes. The power density is $I = P/(\Delta^2\pi/4) = 0.8\ W/cm^2$ and the energy E_e incident on one RBC (diameter $2R_o \approx 8$ μm) is given by $E_e = P(2R_o/\Delta)^2 t = t \times 4 \times 10^{-7}$ W. For t = 1s, this energy value would be 0.4 μJ.

(ii) "scan" mode; the computer-driven mirrors (galvano mirror scanners) of the CLSM allowed to scan the internal Ar^+-ion laser (488 nm, 15 μW) over a raster of 512 × 512 steps. The field of view was irradiated in a point-by-point fashion during the scanning time t_s, which could be varied from 0.5 to 64 s. The step size δ was determined by measuring the number of steps (n = 400) necessary to cover a 100 μm long section of a calibrated micrometer ruler in the focal plane, yielding δ = 100 μm/n = 0.25 μm and a step time of $t_\delta = t_s/512^2$. The "dwell" time τ is defined as the time that the beam remains incident on one erythrocyte (for attached RBC, the cross section A is $A = \pi R_o^2 \approx 50\ \mu m^2$), thus $\tau = Nt_\delta$, where N denotes the number of scanning steps necessary to cover one erythrocyte, $N \approx A/\delta^2 = 800$, so that $\tau = N(1/512^2)t_s = 0.003\ t_s$. The corresponding value E_e is $E_e = P\tau = P \times 0.003\ t_s = t \times 4.5 \times 10^{-8}$ W. For t = 1s, this energy value would be 0.045 μJ.

(iii) "spot" mode; during the irradiation time t, the CLSM galvano mirror scanners were locked at a selected position to irradiate one "point" with an area of w ≈ 0.5 μm diameter, defined by the nearly diffraction-limited spot size of the internal laser. The power density becomes $I = P/(w^2\pi/4) = 7.5\ kW/cm^2$ and $E_e = Pt = t \times 1.5 \times 10^{-5}$ W. For t = 1s, this energy value would be 15 μJ.

For the three modes of irradiation, the laser power P, power density I, and energy E_e, incident on one erythrocyte during irradiation time t (in seconds), are given in Table 2. It should be noted that the irradiation modes are quantified with different accuracies. For example, "field" mode irradiation may vary by about 10% (due to fluctuations in measured power densities and diameter of irradiated area), whereas "spot" mode results depend on individual characteristics of RBC (thickness, age, photoresistance). The "scan" mode is inherently more accurate but for repeated scans, the number of RBC in the field of view may increase during the irradiation time t because of

TABLE 2. Laser Power P, Power Density I, Laser-Beam Dwell Time τ on One Erythrocyte, and Incident Energy E_e on One Erythrocyte, for the Three Modes of Irradiation

Mode	P (W)	I (W/cm^2)	τ (s)	E_e (J/erythrocyte)
field	0.1	0.8	t	$P(2R_0/\Delta)^2 t = 4 \times 10^{-7}$ t
scan	1.5×10^{-5}	7500	$3 \times 10^{-3} t_s$	$P(\tau/t_s)t = 4.5 \times 10^{-8}$ t
spot	1.5×10^{-5}	7500	t	$Pt = 1.5 \times 10^{-5}$ t

sedimentation. The measured value t_h (when 50% of the RBC in the field of view have undergone lysis) will then be too large, since some RBC will have been irradiated during only part of the time t.

Data Acquisition

A single RBC or a region of interest (ROI) containing several (up to 100) RBC was identified in transmission microscopy by illumination with a spectrally-filtered halogen lamp ($\lambda > 500$ nm) or by scanning with the 10-fold attenuated internal laser beam. No observable photodynamic effects were induced during the time needed for ROI selection, focusing, and optical adjustments (e.g., zooming). Fluorescence images were obtained using the "scan" mode, $\lambda_{exc} = 488$ nm (without attenuation of the laser beam) and $\lambda_{fluor} > 560$ nm.

Erythrocytes in an ROI were irradiated for durations t, up to 30 min, to monitor cell lysis. In the "scan" mode, the kinetics of hemolysis could be studied in "real" time by acquiring data at 1 Hz ($t_s = 1$ s). For the "field" and "spot" modes, irradiation was interrupted at intervals 0.5, 1, or 2 min, depending on hemolysis kinetics, and a single "probe" scan ($t_s = 1$ s) with the 10-fold attenuated laser beam provided a transmission image, determining the extent of lysis in the elapsed time interval. Images were stored on optical disk for retrieval, data processing, and evaluation.

Typically, "field" and "scan" mode experiments involved about 100 RBC present in the ROI; exposure was continued until 50% of all RBC were lysed. In the "spot" mode, a selected RBC was exposed for a maximum of 30 min or until lysis was observed. This procedure was repeated on 10 RBC, using each drug and RBC type, both washed and unwashed. All experiments were repeated on three different days, using blood samples from different donors.

RESULTS

Absence of Photothermal Effects

Hemolysis experiments were performed in non-incubated erythrocytes to study possible photothermally mediated effects during microirradiation, using both human and chicken erythrocytes. One hundred cells of each type were irradiated in the "field" and "scan" mode (repeated twice) and 20 cells (of each type) in the "spot" mode. No observable effects where found after exposure for 30 min to either of the three modes of irradiation.

Fluorescence

Both human and chicken erythrocytes showed very weak autofluorescence in the cytosol. Photosensitizer-incubated RBC fluoresced much stronger.

Figure 2 shows fluorescence of unwashed CRBC, incubated for 2 hours with $TPPS_4$, during repeated "scan" mode excitation (scan time of ROI was $t_s = 7$s). Intact cells showed no preferential fluorescence compared to the surrounding solution (frame #1). However, the excitation radiation induced onset of intracellular fluorescence (frames #6–8), particularly in the nucleus (frames #>10). The fluorescence achieved a maximum within 30 scans. Further light exposure (frames #41–60), corresponding to irradiation times t: 280–420 s, resulted in no further change of fluorescence pattern and intensity. This indicates maximal intracellular accumulation of $TPPS_4$ and absence of sensitizer photodegradation. Figure 3, taken after t = 420 s, depicts confocal fluorescence images at 1.0 μm depth resolution, clearly demonstrating that all cytosolic material had leaked from lysed CRBC and that photosensitizer was retained in the nucleus and cellular membrane. In the case of HRBC (Fig. 4), confocal fluorescence images at 1.0 μm depth resolution show that photoinduced intracellular fluorescence, observed after 30 s irradiation, is localized in the cytosolic material and in the membrane. Similar results were obtained with Pd-$TPPS_4$.

Figure 5 shows fluorescence and bright-field transmission images of Photofrin-incubated, unwashed HRBC. Unlike the case of $TPPS_4$ and Pd-$TPPS_4$, in which intact RBC did not fluoresce even after 2 h incubation, Photofrin-incubated

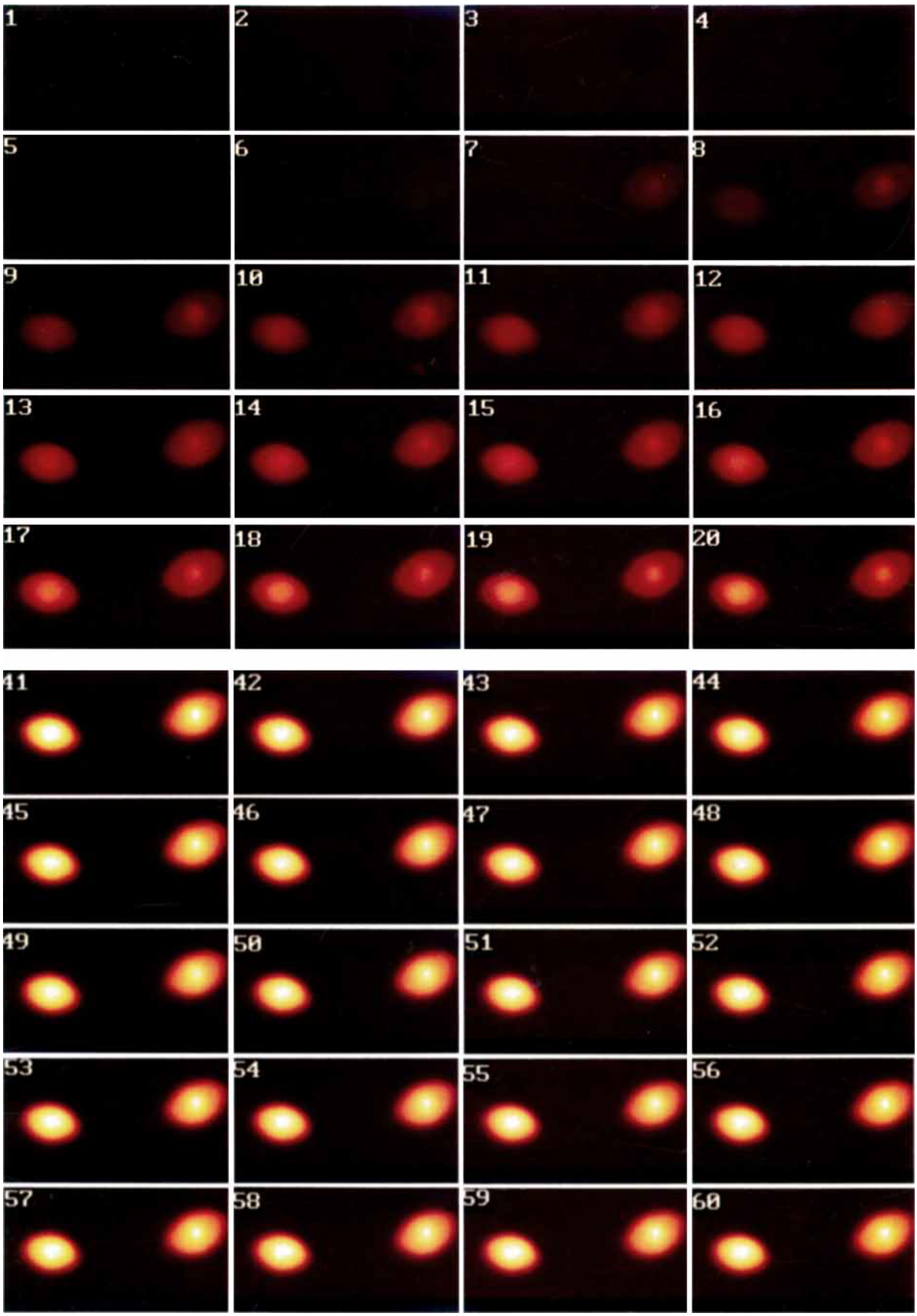

Fig. 2. Temporal evolution of fluorescence in CRBC incubated for 2 h with $TPPS_4$ (10 μg/ml, unwashed). Consecutive frames show images obtained after incremental irradiation for 7 s at 488 nm in the "scan" mode. **Upper panel, frames 1–20; lower panel, frames 41–60.**

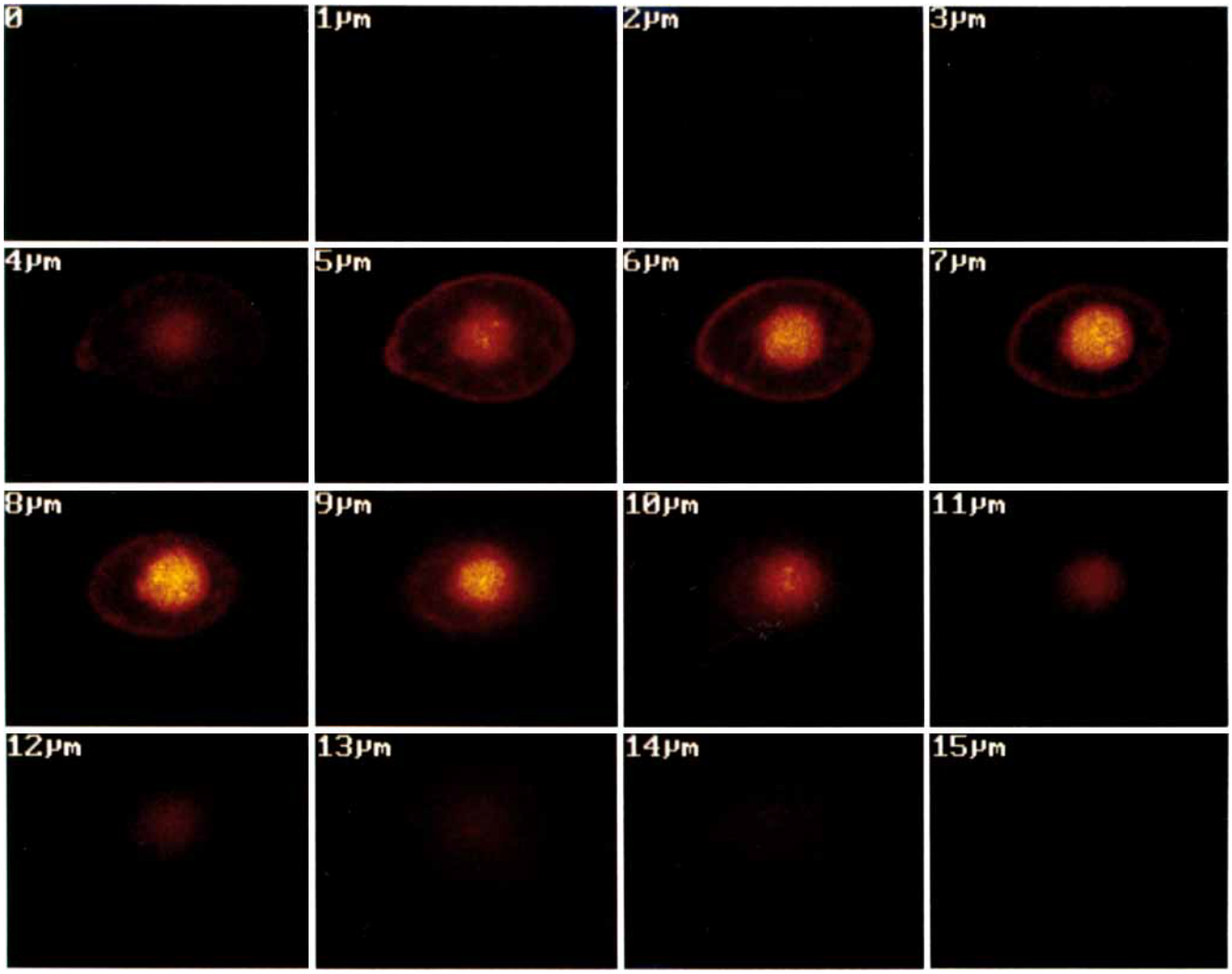

Fig. 3. Depth-resolved fluorescence of $TPPS_4$-incubated CRBC (unwashed) after 420 s irradiation at 488 nm in the "scan" mode; spatial resolution 1.0 μm.

HRBC showed instantaneous fluorescence (panel A). During the short dwell time, $\tau = 6$ ms (Table 2), photosensitizer influx following photoinduced membrane damage is negligible, which means that Photofrin had penetrated the membrane during the 10 min incubation time. Panel B shows that after t = 4 s hemolysis had occurred in 2 out of 10 cells, whereas in panel C (t = 8 s) 80% of cells were hemolyzed. Measurements taken immediately afterwards (panel D) showed persistent fluorescence of Photofrin in lysed cells but, contrary to the case of $TPPS_4$, with reduced intensity. Confocal imaging confirmed that fluorescence originated from ghost membranes (Fig. 6). For Photofrin-incubated CRBC, the temporal evolution of fluorescence is displayed (Fig. 7) by a series of confocal images of the 1.0 μm thick central slice of a CRBC taken at at sequential time intervals of 5 s. Initially, the CRBC showed a homogeneous fluorescence pattern (Fig. 7, panel A); in the course of photohemolysis the cytosolic fluorescence decreased, whereas the nuclear membrane fluorescence increased (panel B). During further exposure the fluorescence reached a maximum followed by a slow decrease (panel C).

MB exhibited strong fluorescence in CRBC, predominantly in the nucleus (Fig. 8), whereas HRBC fluoresced weakly in the membrane. ALA-incubated CRBC did not produce consistent results; only a few randomly distributed erythrocytes present in the ROI showed weak fluorescence. Intercellular dissimilarities are probably due to the different ability of individual erythrocytes to synthesize PP IX.

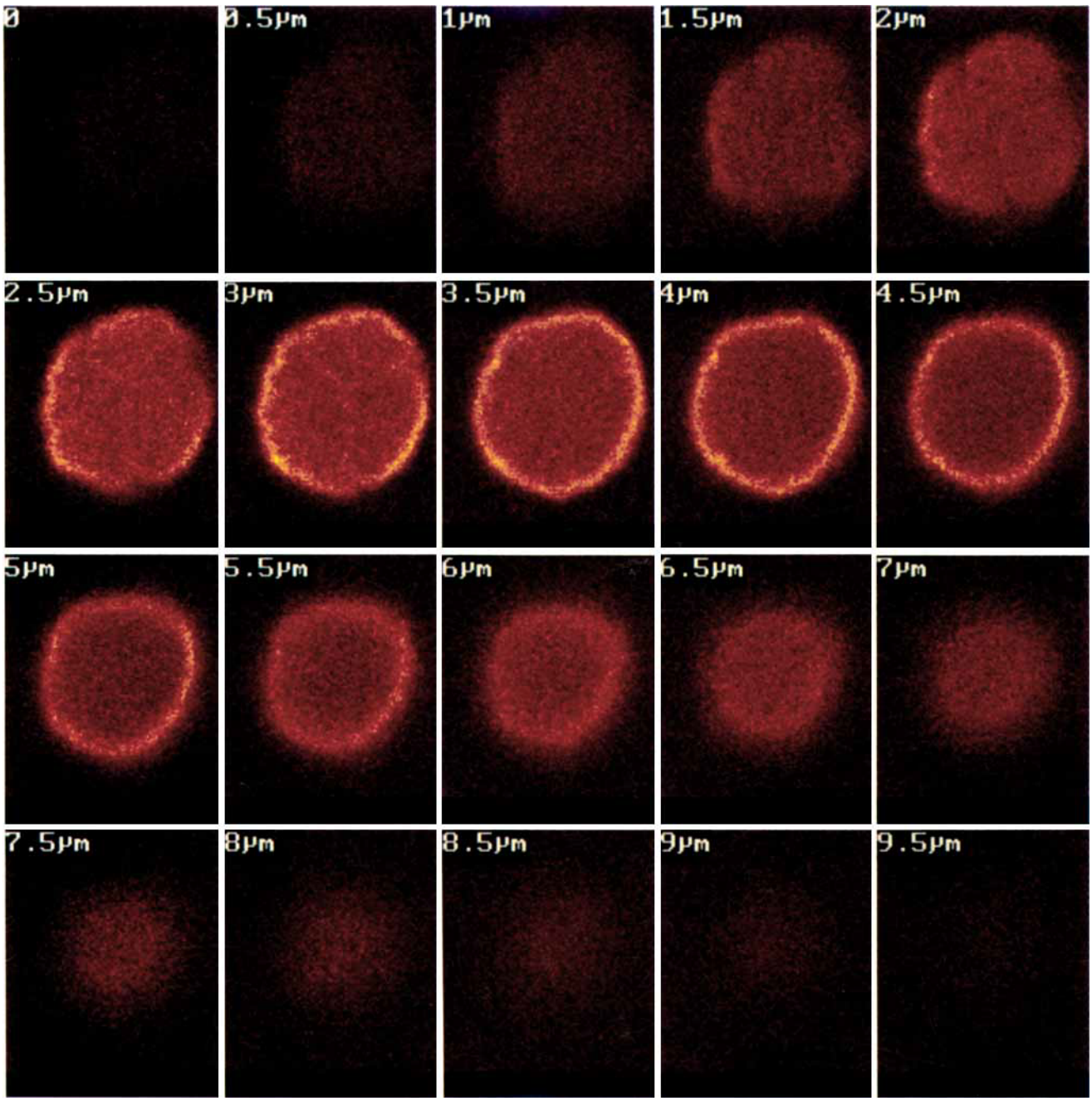

Fig. 4. Depth-resolved fluorescence of $TPPS_4$-incubated HRBC (unwashed) after 30 s irradiation at 488 nm in the "scan" mode; spatial resolution 0.5 μm.

Photodynamic Hemolysis

To study hemolysis, all three irradiation modes for inducing photodamage were used. Strong dissimilarities in hemolysis were observed, probably due to differences in cellular accumulation of the various photosensitizers. Table 3 lists irradiation times to induce hemolysis, t_h, of RBC incubated with different photosensitizers. Irradiation was applied continuous ("field" and "spot" modes) or quasi-continuous ("scan" mode, with t_s = 1 s). Hemolysis was more efficient for unwashed than washed cell suspensions, indicating the important role of extracellular photosensitizing molecules.

A change of morphology, in the absence of light, was observed for Photofrin-incubated

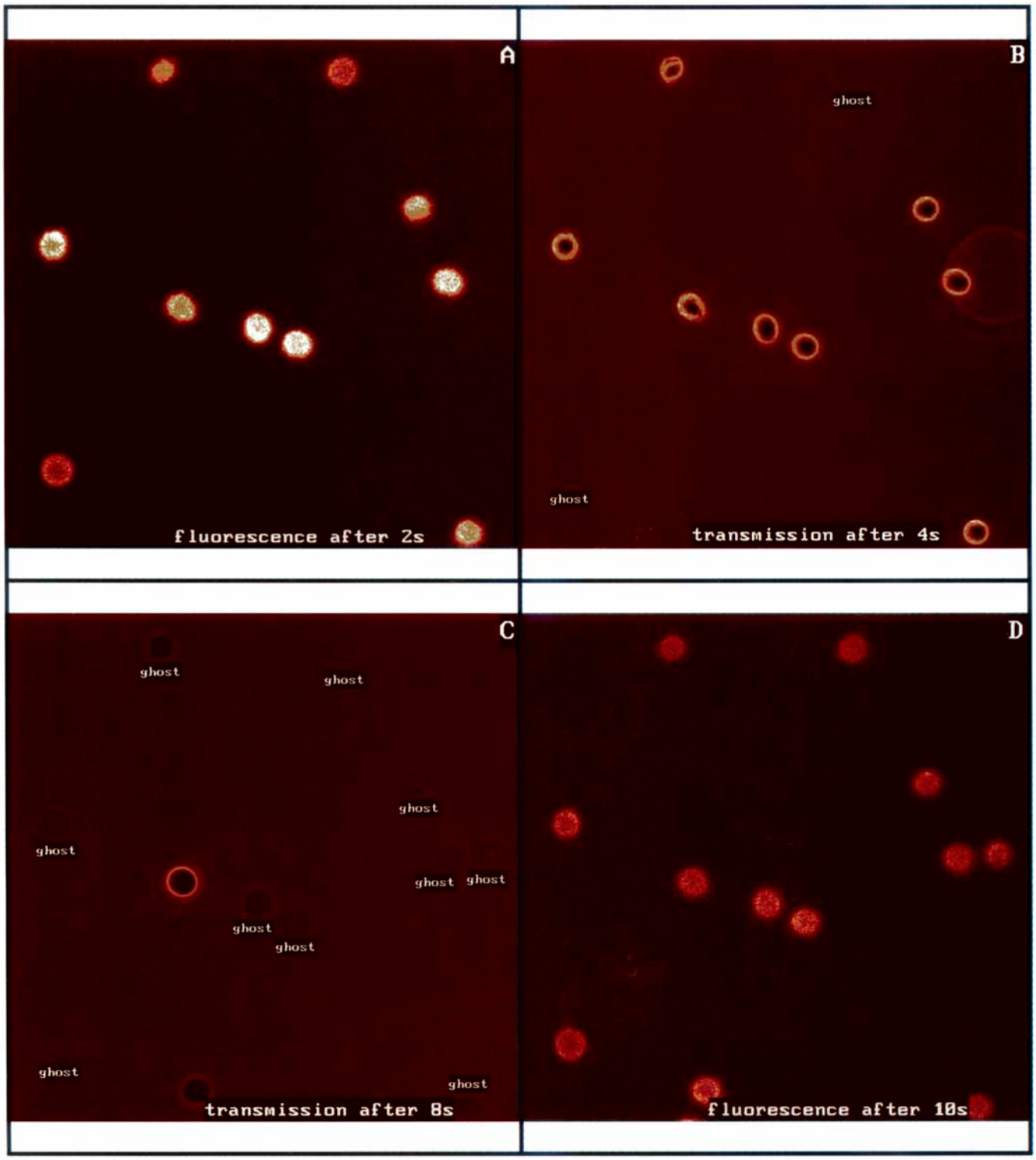

Fig. 5. Fluorescence and transmission images in the "scan" mode (t_s = 2 s) of HRBC incubated for 10 min with Photofrin (10 μg/ml, unwashed). Panel **A:** first scan, fluorescence, t = 2 s; panel **B:** second scan, transmission, t = 4 s; panel **C:** fourth scan, transmission, t = 8 s; panel **D:** fifth scan, fluorescence, t = 10 s.

HRBC, from biconcave to the crenated shape (echinocytes). This supports findings from Ben-Hur et al. [4]. The ellipsoidal CRBC shape did not change in the dark. In all cases, however, light-induced changes in morphology were observed prior to photohemolysis. These included transfor-

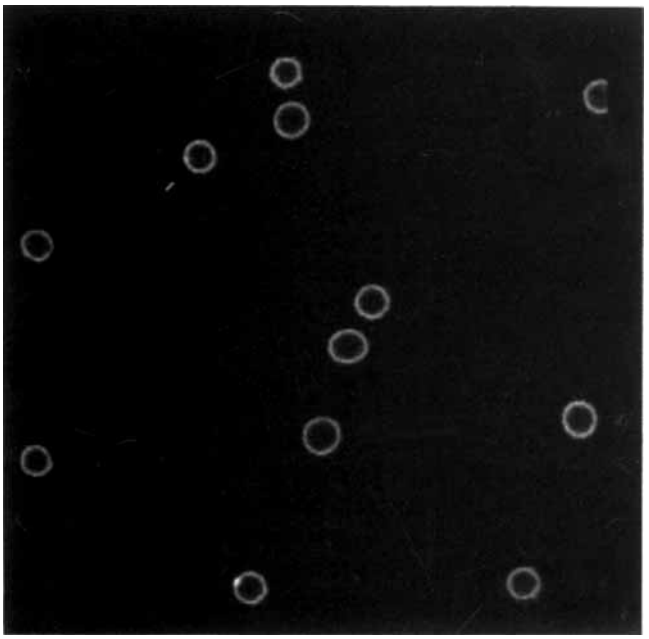

Fig. 6. Confocal fluorescence image of unwashed HRBC incubated for 10 min with Photofrin (10 μg/ml) after lysis.

mation of the characteristic biconcave profile of HRBC to a spherical one, rounding (for crenated HRBC) and swelling (about 20% increase in volume); CRBC became "folded" and developed microdefects in the exterior membrane (Fig. 9).

Entries in Table 3 can be transformed into "apparent" threshold energies E_e by multiplying t_h with the corresponding conversion factor in Table 2, column 5. It should be noted that E_e, obtained under continuous irradiation conditions, is larger than the "real" threshold energy E_{th}, because of the time required for "dark" reactions (involving efflux of hemoglobin, subsequent to irreversible membrane damage). The exact value E_{th} = 2 μJ/erythrocyte (for Photofrin and HRBC) was determined by reducing the incident radiant energy, delivered in the "scan" mode, and probing the field of view after "dark" intervals of 10 min and establishing at which incident energy 50% of the RBC in the irradiated field were hemolyzed. The presence of dark reactions at threshold energies was demonstrated by exposing Photofrin-incubated HRBC to a slow "scan" mode, delivering sufficient radiant energy to induce hemolysis in just one scan (t_s = 64 s, τ = 0.2 s), as observed by subsequent imaging with a fast (t_s = 1 s) and weak (attenuated to 10%) probe scan. Figure 10 shows hemolysis in the upper part of the irradiated field (where the "dark" time was longest, see Discussion), whereas the lower part of the field (that had received identical radiant exposure) did not exhibit hemolysis.

It is interesting to note that with ALA incubation it was possible to lyse an individual CRBC (using the "spot" mode) by preselecting a fluorescing CRBC, which apparently had synthesized detectable amounts of porphyrin fluorophores from exogenous ALA, whereas non-fluorescing CRBC were resistant to photohemolysis.

DISCUSSION

Laser microbeam irradiation was employed, for the first time, to study photodynamic cell damage. We found that low-power microbeams used in laser scanning microscopy are an efficient source to induce photohemolysis in sensitized erythrocytes, and to allow simultaneous confocal fluorescence imaging. The effects of intracellular spot irradiation as well as of a scanning microbeam were compared with macrobeams ("field mode").

The microbeam induces hemolysis based on photochemical reactions, and not on thermal damage. The absence of photothermal effects can be illustrated by the following estimate for the temperature rise due to "spot" mode irradiation.

The decadic absorption coefficient of hemoglobin [16], α (488 nm) = 44 cm^{-1}, is much larger than that of the photosensitizers at the relevant concentrations, α (488 nm) = 0.0036 cm^{-1} (see Table 1). Consider a spherical RBC, as observed in hypotonic solution (diameter $2R_o$ = 8 μm), and assume the microbeam (diameter 0.5 μm) traverses the RBC along a main axis, so that the optical path is 0.0008 cm. The heat flow per unit time Q_{in} into the RBC is determined by the absorbed radiant intensity

$$\begin{aligned} Q_{in} &= P[1 - \exp(-2.3 \times \alpha \times 2R)] \\ &= P[1 - \exp(-2.3 \times 44 \times 0.0008)] \\ &\approx P \times 0.078 \end{aligned} \quad (1)$$

The heat flow out of the uniformly heated RBC into the surrounding solution is [17]

$$Q_{out} = 4\pi R^2 q(R) \quad (2)$$

For steady state conditions

$$q(R) = \kappa \Delta T/R$$

where κ = 0.6 W/mK denotes the thermal con-

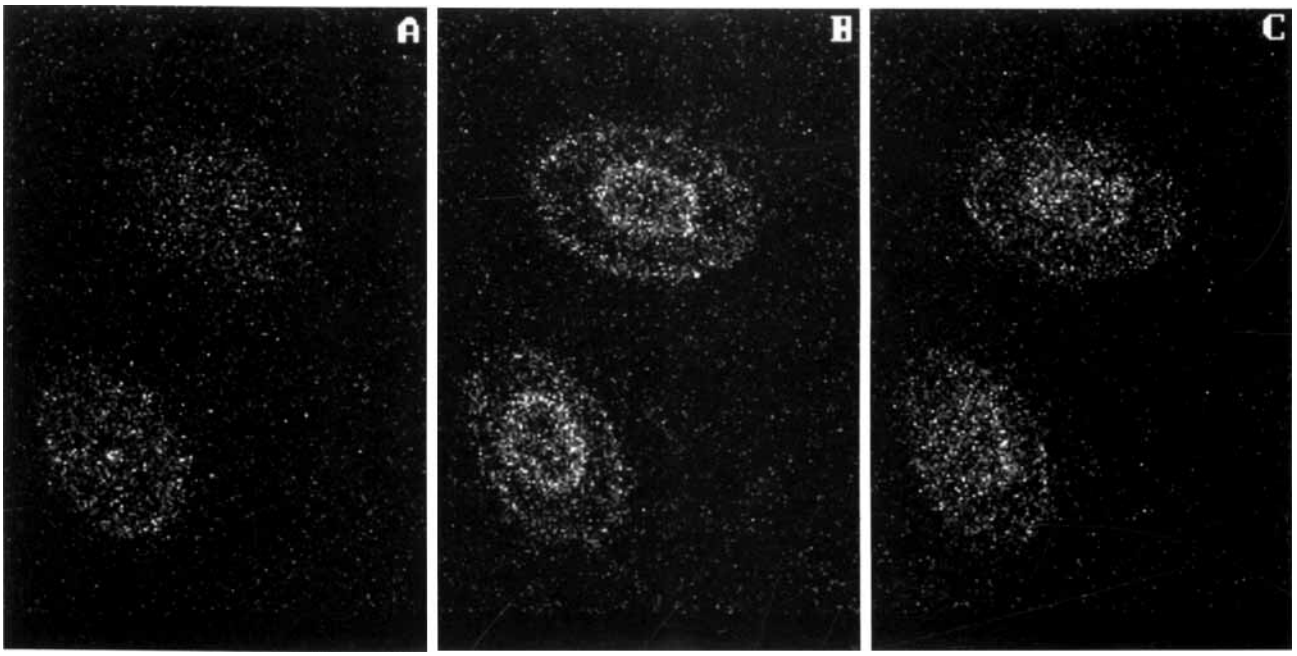

Fig. 7. Confocal fluorescence images of the 1.0 μm thick central slice of CRBC incubated for 10 min with Photofrin (10 μg/ml, unwashed) taken at time intervals of 5 s. Panel **A:** first scan; panel **B:** scan 6; panel **C:** scan 12.

ductivity (taken to be equal to that of water), and ΔT is the temperature rise due to Q_{in}. Thus

$$Q_{out} = 4\pi R\kappa\Delta T$$

At equilibrium, $Q_{in} = Q_{out}$

$$P \times 0.078 = 4\pi R\kappa\Delta T$$

$$\Delta T = 0.078 \times 15 \times 10^{-6}/4\pi \times 4 \times 10^{-6} \times 0.6 \approx 0.04\ ^\circ C \quad (3)$$

Therefore, photothermal effects are negligible and are not responsible for lysis observed with RBC incubated with photosensitizers, as described in the following sections.

Uptake and PDT-induced redistribution of sensitizer was monitored using fluorescence techniques. Intact CRBC, incubated with $TPPS_4$ or Pd-$TPPS_4$, did not fluoresce. However, fluorescence was observed after the external membrane had been damaged (Figure 2, frames #7 and higher, $t > 50$ s) as a consequence of irradiation, with (Table 2) $E_e = P(\tau/t_s)\, t \geq 4.5 \times 10^{-8} \times 50 \geq 22$ μJ/erythrocyte. Onset of fluorescence may be interpreted by influx of $TPPS_4$ through the membrane, indicating a photodynamic induced higher permeability. In addition, preferential binding to cytosolic proteins increases $TPPS_4$ fluorescence [18]. Moreover, at the high concentrations used for fluorescence measurements ($> 10^{-5}$ M), $TPPS_4$ forms aggregates [19], accompanied by a reduced quantum yield for fluorescence, so that monomerization in the cytoplasm increases the fluorescence intensity. The combined influences of preferential accumulation [18], increased fluorescence of protein-bound molecules [20], and monomerization [19] may account for the observations in Figure 2. The type and charge of proteins on the external surface of the cell membrane are distinctly different from those on the internal surface. 2 h incubation caused insufficient binding to the (negatively charged) external membrane to result in measurable fluorescence. However, after permeating through the injured membrane, $TPPS_4$ molecules became attached to the internal surface of the cell membrane, as demonstrated in Figures 3 and 4. This hypothesis is corroborated by the fact that washed RBC, where excess porphyrin had been removed, showed only weak cellular fluorescence, indicating the important role of free $TPPS_4$ molecules present in the PBS solution.

The hydrophobic constituents of Photofrin are known to penetrate easily into cells [21] resulting in cellular fluorescence that, unlike for

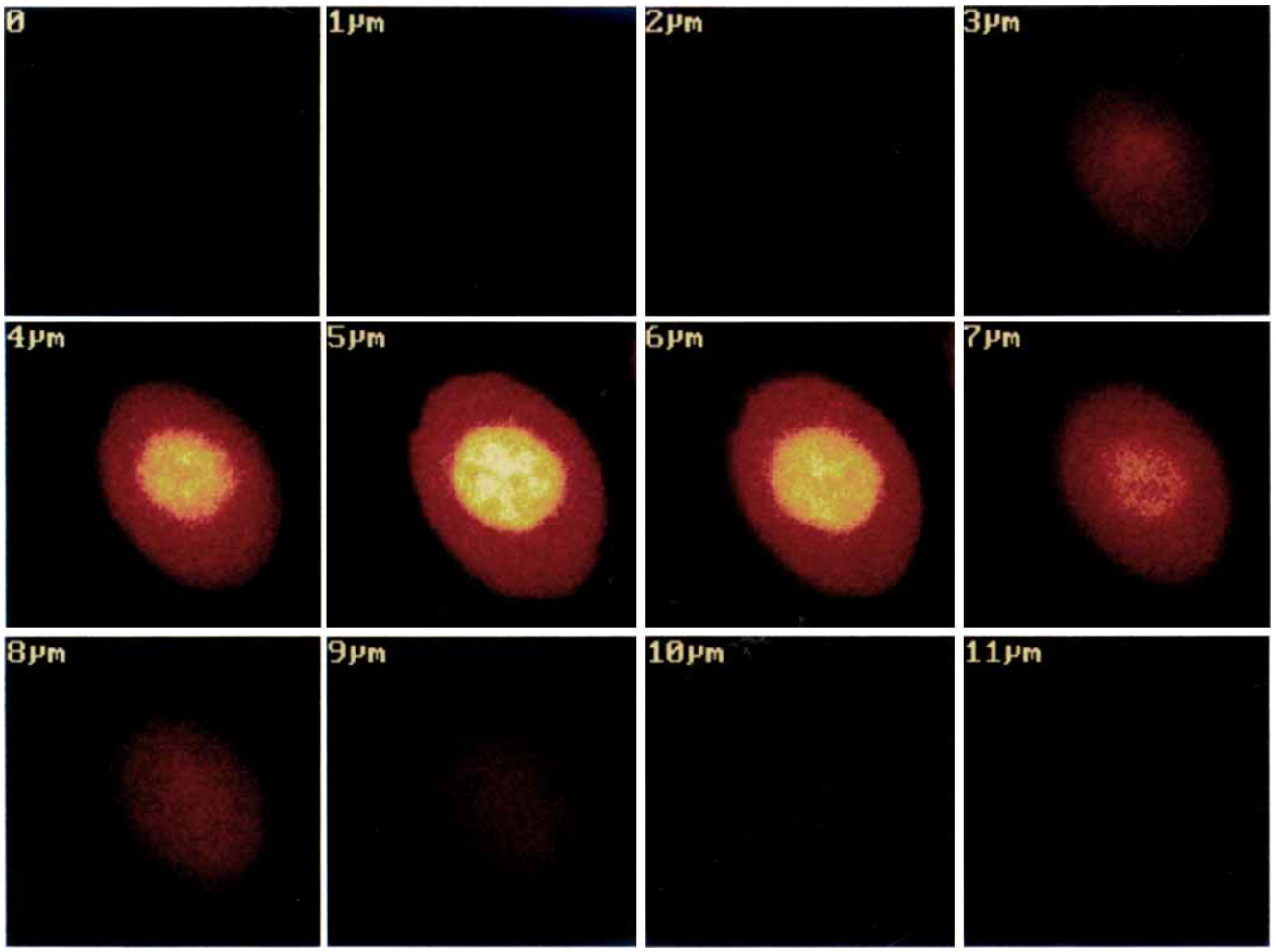

Fig. 8. Depth resolved fluorescence of unwashed CRBC incubated for 2 h with methylene blue (resolution 1.0 μm, unwashed). Note intranuclear fluorescence pattern.

$TPPS_4$, does not necessitate prior photoinduced membrane damage (Fig. 5a). The fact that in unwashed cell suspensions intracellular fluorescence intensity was larger than extracellular may be due to a combination of the same three factors mentioned above for $TPPS_4$: preferential binding to intracellular proteins, higher fluorescence quantum yield, and monomerization. The fluorescence decrease observed during continued irradiation, even for lysed cells, must be ascribed to photodegradation [22,23]. Lysis alone (efflux of cytoplasmatic material) is apparently not sufficient to explain the lower fluorescence intensity, as shown in our studies with $TPPS_4$ where persistent fluorescence was observed (Fig. 2) even after prolonged irradiation when cells had been lysed completely.

Methylene blue [24] was different from other photosensitizers in that it showed strong fluorescence in intact CRBC, which can be explained by the preferential localization of hydrophilic photosensitizers in the nucleus [25].

ALA-incubated cells exhibited weak fluorescence in randomly distributed CRBC proving that porphyrin biosynthesis [14] must have taken place. It is known that mitochondria in nucleated mammalian cells are essential in the biosynthesis of PP IX [26]. Our fluorescence results indicate that an isolated, mitochondria-free nucleated avian cell can also synthesize porphyrins. This is in agreement with early studies of ALA-incubated CRBC, where porphyrins were detected spectroscopically after extraction from CRBC [27].

Based on standard dosimetry considerations, it may be thought that, for a given photosensi-

TABLE 3. Irradiation Times (t_h/min) to Induce Hemolysis[a]

		HRBC		CRBC	
Sensitizer	Mode	Unwashed	Washed	Unwashed	Washed
Photofrin	field	1.5	3.5	3.5	11
	scan	2	4.5	7	12
	spot	0.15*	1*	0.6*	4*
MB	field	>>30	>>30	10	15
	scan	>>30	>>30	~20	>30
	spot	>>30	>>30	2*	8*
$TPPS_4$	field	7	>>30	ca. 10	>>30
	scan	13	>>30	27	>>30
	spot	2.5*	4	3*	5
Pd-TPPS	field	8	>>30	/	/
	scan	6	>>30	13	>>30
	spot	1.5*	2.3	2.5*	4
ALA	field	/	/	/	/
	scan	>>30	/	>>30	/
	spot	>>30	/	3->>30	/

[a]In "field" and "scan" modes, t_h refers to time necessary to lyse 50% of irradiated RBC. The symbol * indicates that the Ar^+-laser was attenuated 10-fold; >30: number of lysed cells after t_h = 30 min was between 5% and 50%; >>30: number of lysed cells after t_h = 30 min was <5%.

tizer, different irradiation modes would cause RBC hemolysis in times, t_h, that would be inversely proportional to the corresponding incident energies E_e, defined in Table 2:

$$t_h(\text{field}) : t_h(\text{scan}) : t_h(\text{spot}) = 1/E_e(\text{field}) : 1/E_e(\text{scan}) : 1/E_e(\text{spot}) = 1 : 9 : 0.03. \quad (4)$$

Measured values of t_h in the three irradiation modes listed in Table 3 are qualitatively consistent with this simplified model. For a given photosensitizer, t_h ratios deviate by less than one order from theoretical predictions. This may be caused by a variety of effects such as sensitizer photostability, intracellular localization, and dependence of singlet oxygen quantum yield on the microenvironment [18]. The observed discrepancies may be explained by considering: (a) photodegradation: this is expected to produce relatively less lysis in the "spot" mode, since the minute quantity of drug, locally excited with high radiant energy density, quickly photodegrades to less active photoproducts [23]. (b) drug localization: for membrane-bound drugs, the total amount of sensitizer present in the microscopic area irradiated in the "spot" mode, $\pi(0.5/2)^2 = 0.2\mu m^2$, is not always sufficient to cause irreversible membrane damage since less than 1% of the RBC membrane area, A = 50 μm^2, is affected. For internalized drugs, the position of the beam spot did not always coincide with the region of maximum intracellular drug localization. (c) dark reactions: irradiation damage initiates cellular efflux/influx which causes hemolysis and continues even in the dark. In the "field" and "spot" modes, hemolytic reactions occur during irradiation. In the "scan" mode, dark periods between consecutive irradiations are $t_s/\tau(512^2/800) = 330$ times longer than dwell times (Table 2) so that lysis proceeds in the dark, making the "scan" mode appear to be more efficient.

The influence of dark reactions was investigated by setting the "scan" time t_s = 64 s (sufficient to cause hemolysis in one single scan), followed by a quick "probe" scan (t_s = 1 s); in addition, 2 s is needed for (manual) switching of irradiation conditions. The hemolytic irradiation of a single HRBC, lasting $\tau = 64/330 = 0.2$ s, is separated from the subsequent probe scan by a dark interval, the duration of which depends on the Y coordinate in the field of view. A given spot, with area $\pi(0.5/2)^2 = 0.2\ \mu m^2$, in an RBC situated in the uppermost segment of the field of view is probed 66 s after hemolytic irradiation, whereas a similar spot in an RBC situated in the lowermost segment is probed 3 s after irradiation. If we consider the time interval between the completed irradiation of a whole RBC situated in the top segment and an RBC situated in the bottom segment of the field of view, the dark time is reduced at each end by $(t_s \times d)/(\delta \times 512) = 64 \times 8/(0.25 \times 512) = 4$ s, leaving still a net dark period of 66-(2 × 4) = 58 s. The occurrence of dark reactions can thus be studied in the "scan" mode, simply by monitoring lysis as a function of Y (Fig. 9).

For Photofrin-incubated HRBC, the real threshold energy E_{th} = 2 μJ/erythrocyte, given in the Results (which fully allowed for dark reactions, up to 600 s), should be compared with the apparent threshold energy, corresponding to hemolytic irradiation (about 50% cell lysis in Fig. 9), with t_s = 64 s, E_{th} = 15 μ W × 0.2 s = 3 μJ/erythrocyte (which partially allowed for dark reactions, up to 66 s), and the incident energy deduced from t_h in Table 3, $E_e = 15\mu W \times 0.003 \times 120s = 5.4$ μJ/erythrocyte (which allowed for cumulative dark reactions, probably accompanied by membrane repair reactions, during the 120 intermittent off-periods of 1 s each between consecutive scans).

For a given photosensitizer, effects (a) and (b) above may cause the "spot" mode to be less efficient relative to the standard "field" mode results (i.e., t_h[spot] may become larger than pre-

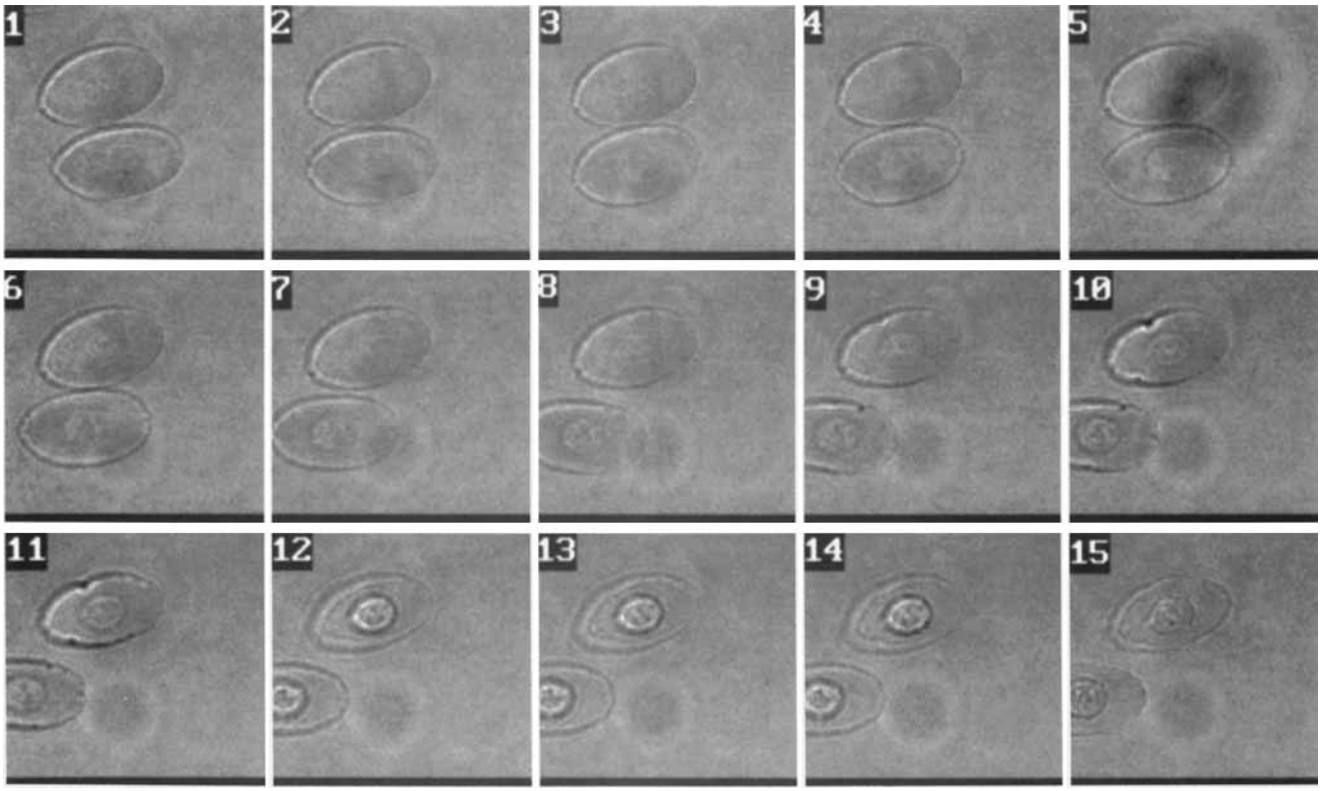

Fig. 9. Transmission images of a pair of unwashed CRBC during the course of photohemolysis (scans 1–15). First microdefects appear (scans **8–11**), followed by efflux of hemoglobin (scans **12–15**).

dicted by dosimetry considerations, c.f. Eq. 4). However, Table 3 shows that typical values for t_h(spot)/t_h(field) range from 0.01 (for Photofrin) to 0.036 (for $TPPS_4$) and are therefore of the same order as the predicted ratio of 0.03, given in Eq. 4. In contrast, effect (c) will cause the "scan" mode to be relatively more efficient than the standard "field" mode (thus making t_h[scan] smaller than predicted); indeed t_h(scan)/t_h(field) $\approx$ 2 (Table 3), instead of the predicted ratio 9 in Eq. 4.

When comparing efficiencies of different photosensitizers, specific considerations prevail for each irradiation mode and sample procedure. As an example, we present (Fig. 11) a comparison of PDT efficacy of photosensitizers, based on Table 3, limited to the "scan" mode and to unwashed RBC. Photofrin was the most efficient photosensitizer and ALA the least efficient. CRBC were more resistant to PDT than HRBC, except for the case of MB. Other irradiation modes used to induce hemolysis lead to a different ranking of photosensitizers; cross correlations between various combinations of photosensitizers/irradiation-modes were not attempted.

In conclusion, CSLM instrumentation pro-

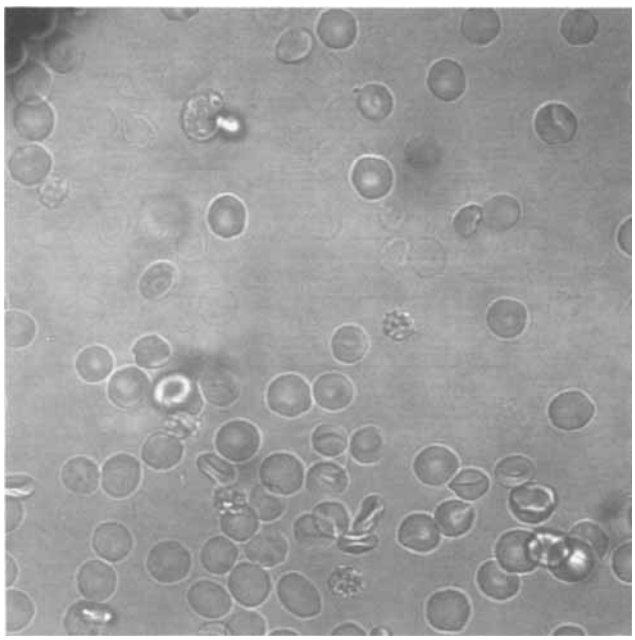

Fig. 10. Transmission image of HRBC incubated for 10 min with Photofrin (10 μg/ml, unwashed) and hemolysed in one scan with t_s = 64 s. The presence of lysed cells (about 50%), mainly in the upper part of figure, is due to dark reactions.

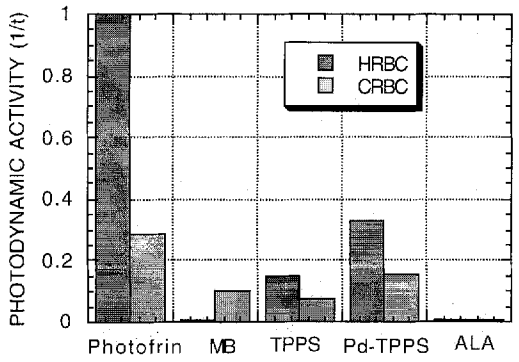

Fig. 11. Relative efficacy (expressed as $1/t_h$) of photosensitizers to hemolyse erythrocytes (using the "scan" mode).

vided a convenient source for microirradiation with sufficient power, at a selected wavelength, to induce (sub)cellular effects. In addition, the unique properties of CSLM allowed study of the pharmacokinetics (on a time scale of seconds/minutes—by observing temporal evolution of fluorescence) and the spatial distribution of fluorophores (by depth resolved imaging).

Human erythrocytes are relatively simple structured model systems for studying membrane characteristics, whereas avian erythrocytes allow study of nuclear effects. As we have shown, the physical-chemical properties of a photosensitizer determine its efficacy in photohemolysis. This, in turn, has bearing on the mechanism of PDT. For example, hydrophobic Photofrin easily penetrates through the cellular membrane of RBC and, upon excitation by light, instantaneously becomes cytotoxic. Therefore, when introduced intravenously, Photofrin will first act on RBC. Depending on Photofrin pharmacokinetics, PDT-induced vascular damage will occur and has mainly to be considered in phototreatment with low time periods between injection and light exposure. The damage will be less significant with decreasing sensitizer-levels in blood. In contrast, anionic $TPPS_4$ does not penetrate the negatively charged membrane of intact RBC. Hence vascular effects due to altered RBC morphology are less likely to occur. The cationic, hydrophilic compound MB was seen to be mainly active in the CRBC nucleus (in accordance with its well-known binding to nucleic acids). Hence, HRBC do not constitute primary targets for MB-PDT. Obviously, ALA too is not expected to induce vascular photodynamic effects through hemolysis, even though ALA-induced vascular damage may occur due to cytotoxic effects in endothelial cells.

ACKNOWLEDGMENTS

This work was supported by NIH Biomedical Resource Technology Program grant RR01192 and by grant 93-00154 of the US-Israel Binational Science Foundation (BSF). The authors thank Dr. T. Krasieva for helpful discussions regarding fluorescence microscopy. K.K. acknowledges financial support from the Deutsche Forschungsgemeinschaft (DFG).

REFERENCES

1. Tromberg BJ, Orenstein A, Kimel S, Barker SJ, Hyatt J, Nelson JS, Berns MW. In vivo tumor oxygen tension measurements for the evaluation of the efficiency of photodynamic therapy. Photochem Photobiol 1990; 52:375–385.
2. Star WM, Marijnissen JPA, van den Berg-Blok AE, Versteeg AAC, Franken NAP, Reinhold AS. Destruction of rat mammary tumor and normal tissue microcirculation by hematoporphyrin derivative photoradiation observed in vivo in sandwich observation chambers. Cancer Res 1986; 46:2532–2540.
3. Nelson JS, Liaw LH, Orenstein A, Roberts WG, Berns MW. Mechanism of tumor destruction following photodynamic therapy with hematoporphyrin derivative, chlorin, and phthalocyanine. J Natl Cancer Inst 1988; 80:1599–1605.
4. Ben-Hur E, Orenstein A, Livne A, Rosenthal I. Photosensitized oxidation of human red blood cells: cation effects on volume changes and relevance to blood vessel occlusion. Lasers Life Sci 1990; 3:255–262.
5. Deuticke B, Henseleit U, Haest CW, Heller KB, Dubbelman TMAR. Enhancement of transbilayer mobility of a membrane lipid probe accompanies formation of membrane leaks during photodynamic treatment of erythrocytes. Biochim Biophys Acta 1989; 982:53–61.
6. König K, Kunzi-Rapp K. On-line measurement of photodynamically induced lysis of erythrocytes with and without nucleus by small angle light scattering and video-intensified microscopy. In: Waidelich W, Waidelich R, Hofstetter A, eds. "Laser in Medicine 1993." Berlin: Springer Verlag 1994, pp 91–99.
7. Lev B, Hanania J, Malik Z. Morphological deformations of erythrocytes induced by hematoporphyrin and light. Lasers Life Sci 1993; 5:219–230.
8. Reed MWR, Wieman TJ, Schuschke DA, Tseng MT, Miller FN. A comparison of the effects of photodynamic therapy on normal and tumor blood vessels in the rat microcirculation. Radiation Res 1989; 119:542–552.
9. Gottfried V, Lindenbaum ES, Kimel S, Hammer-Wilson MJ, Berns MW. Laser photodynamic therapy of cancer: the CAM model for measuring damage to blood vessels in-vivo. Proc SPIE 1990; 1442:218–229.
10. Fingar VH, Wieman TJ, Wiehle SA, Serrito P. The role of microvascular damage in photodynamic therapy: the effect of treatment on vessel constriction, permeability and leucote adhesion. Cancer Res 1992; 52:4914–4921.
11. Hilf R. Cellular targets of photodynamic therapy as a guide to mechanism. In: Henderson BW, Dougherty TJ, eds. "Photodynamic Therapy—Basic Principles and Clin-

ical Applications." New York: Marcel Dekker Inc, 1992, pp 47–54.
12. Henderson BW, Dougherty TJ. How does photodynamic therapy work? Photochem Photobiol 1992; 55:145–157.
13. Wilson DF. Oxygen dependent quenching of phosphorescence: a perspective. In: Erdmann W, Bruley DF, eds. "Oxygen Transport to Tissue XIV." New York: Plenum Press, 1992, pp 195–201.
14. Kennedy JC, Pottier RH. Endogenous protoporphyrin IX, a clinically useful photosensitizer for photodynamic therapy. J Photochem Photobiol B 1992; 14:275–292.
15. König K, Kienle A, Boehncke W-H, Kaufmann R, Rück A, Meier T, Steiner R. Photodynamic tumour therapy and on-line fluorescence spectroscopy after ALA administration using 633 nm-light as therapeutic and fluorescence excitation radiation. Opt Eng, 1994; 33(9):2945–2952.
16. van Gemert MJC, Welch AJ, Miller ID, Tan OT. Can physical modeling lead to an optimal laser treatment and strategy for port-wine stains? In: Wolbarsht ML, ed. "Laser Applications in Medicine and Biology," vol 5. New York: Plenum Press, 1991, pp 199–275.
17. Carslaw HS and Jaeger JC. "Conduction of Heat in Solids." Oxford: Clarendon, 1959.
18. Gottfried V, Peled D, Winkelman JW, Kimel S. Photosensitizers in organized media: singlet oxygen production and spectral properties. Photochem Photobiol 1988; 48: 157–163.
19. Ribo JM, Crusats J, Farrera JA, Valero ML. Aggregation in water solutions of tetrasodium diprotonated meso-tetrakis(4-sulfonatophenyl)porphyrin. J Chem Soc, Chem Commun 1994:681–682.
20. Winkelman JW, Arad D, Kimel S. Stereochemical factors in the transport and binding of photosensitizers in biological systems and in photodynamic therapy. J Photochem Photobiol B 1993; 18:181–189.
21. Roberts WG, Berns MW. In vitro photosensitization I. Cellular uptake and subcellular localization of mono-L-aspartyl chlorin e_6, chloro-aluminum sulfonated phthalocyanine, and Photofrin II. Lasers Surg Med 1989; 9:90–101.
22. König K, Schneckenburger H, Rück A, Steiner R. In vivo photoproduct formation during PDT with ALA-induced endogenous porphyrins. J Photochem Photobiol B 1993; 18:287–290.
23. Moan J. Effect of bleaching of porphyrin sensitizers during photodynamic therapy. Cancer Lett 1986; 33:43–53.
24. König K, Bockhorn V, Dietel W, Schubert H. Photochemotherapy of animal tumors with the photosensitizer Methylene Blue using a krypton laser. Cancer Res Clin Oncol 1987; 113:301–303.
25. Rück A, Köllner T, Dietrich A, Strauss W, Schneckenburger H. Fluorescence formation during photodynamic therapy in the nucleus of cells incubated with cationic and anionic water-soluble photosensitizers. J Photochem Photobiol B 1992; 12:403–412.
26. König K, Schneckenburger H, Walt H, Leemann T, Wyss-Desserich MT, Rück A, Tromberg BJ. Microscopic Studies on ALA-incubated tumor cells and tumor spheroids. SPIE-Proceedings 2133: Optical Methods for Tumor Treatment and Detection, 1994; 238–248.
27. Dresel EIB, Falk JE. Studies on the biosynthesis of blood pigments. Biochem J 1956; 63:72–79.